

Article

# Icariin-Functionalized Coating on TiO<sub>2</sub> Nanotubes Surface to Improve Osteoblast Activity In Vitro and Osteogenesis Ability In Vivo

Aobo Ma , Haiyan Shang, Yunjia Song, Bo Chen, Yapeng You, Wen Han, Xu Zhang, Wenyi Zhang, Ying Li \* and Changyi Li \*

School of Dentistry, Tianjin Medical University, Tianjin 300070, China; maaobo@tmu.edu.cn (A.M.); shanghaiyan@tmu.edu.cn (H.S.); songyunjia@tmu.edu.cn (Y.S.); chenbo@tmu.edu.cn (B.C.); youyapeng@tmu.edu.cn (Y.Y.); hanwen@tmu.edu.cn (W.H.); zhangxu@tmu.edu.cn (X.Z.); zhangwenyi@tmu.edu.cn (W.Z.)

\* Correspondence: yingli@tmu.edu.cn (Y.L.); lichangyi@tmu.edu.cn (C.L.); Tel.: +86-22-23332034 (Y.L.)

Received: 24 April 2019; Accepted: 15 May 2019; Published: 18 May 2019



**Abstract:** Surface modification of titanium is encouraged to facilitate early osseointegration in dental and orthopedic fields. Icariin is the main active constituents of *Herba Epimedii*, which has good bone-promoting ability. We established an icariin-functionalized coating composed of icariin and poly (lactic-co-glycolic acid) (PLGA) on TiO<sub>2</sub> nanotubes surface (NT-ICA-PLGA) to promote osteoblast cell activity and early osseointegration. Surface topography, wettability and drug release pattern of the established NT-ICA-PLGA surface were characterized by scanning electron microscopy (SEM), contact angle test and drug release test. MC3T3-E1 osteoblast cell activity tests were performed using SEM, immunofluorescent staining, cell counting kit-8 and alkaline phosphatase assays. The osteogenic effects of different surfaces were observed using a rat model. Surface characterization proved the successful fabrication of the icariin-functionalized coating on the TiO<sub>2</sub> nanotube structure, with increased wettability. The NT-ICA-PLGA substrate showed sustained release of icariin until two weeks. Osteoblast cells grown on the NT-ICA-PLGA substrate displayed improved cell adhesion, proliferation and differentiation ability than the control Ti surface. The in vivo experiment also revealed superior bone forming ability on the NT-ICA-PLGA surface, compared to the pure Ti control. These results imply that the developed NT-ICA-PLGA substrate has a promising future use as functionalized coating for implant surface modification.

**Keywords:** icariin; TiO<sub>2</sub> nanotubes; PLGA coatings; controlled-release; titanium; surface modification; osteogenesis

## 1. Introduction

Titanium and titanium alloys are the most widely used materials in dental implants due to their outstanding features, which exhibit an appropriate combination of mechanical properties and biocompatibility [1]. However, the bioinertness of untreated Ti implants impaired the initial cell adhesion and bone integration, resulting in delayed osseointegration and even implant failure [2]. In order to solve these problems, surface modification has been considered to be an effective way to promote bone bonding of implants. Different surface modification methods include physical methods (sandblasting, plasma spraying, emerging technology of three-dimensional printing to create micro-architected and nano-architected surface topography, and plasma spraying), chemical methods (anodizing, etching, alkali treatment) and biological methods (functional proteins, growth factors, peptides) [3–5]. In recent years, TiO<sub>2</sub> nanotubes generated by an electrochemical anodization technique

have drawn wide attention owing to its outstanding biocompatibility compared with conventional Ti implant and potential drug delivery application [6]. Besides, these nano-porous structures are fabricated by economical processes and embody many advantages, such as pore controllability, evenness of pore distribution, high surface area, high loading capability, chemical stability, mechanical rigidity and excellent biocompatibility [7]. Several studies have demonstrated that the surface morphology of TiO<sub>2</sub> nanotubes could improve adhesion, proliferation, and differentiation of osteoblast cells and mesenchymal stem cells (MSCs) [8,9]. In order to fabricate the novel implant material, it is essential to construct biomimetic microenvironments on the surface by incorporating osteogenic substance with nano-scale topography of TiO<sub>2</sub> nanotubes. Herein, we loaded icariin (ICA, the main active ingredient of herba epimedii) into TiO<sub>2</sub> nanotubes, which also serves as a drug delivery system. At present, combining bone implants with traditional Chinese medicine has become a research hotspot. Icariin has been widely used in clinic for the reason that it may improve the proliferative activity of osteoblasts and inhibit the formation of osteoclasts, especially in the treatment of osteoporosis [10]. Meanwhile, the combination of icariin and a helioxanthin-derived small compound can also induce the osteogenic differentiation in vitro to a similar level with the effect of bone morphogenetic protein-2. In addition, icariin is a promising anabolic compound, applied in bone tissue engineering [11]. It is shown that icariin could accelerate bone formation and suppress bone absorption. Although TiO<sub>2</sub> nanotube is regarded as a drug delivery carrier, undesired burst release of drug occurs often. Thus, numerous studies have analyzed the release of different kinds of drugs by TiO<sub>2</sub> nanotubes and provided many strategies to achieve long-term release of drugs from the TiO<sub>2</sub> nanotubes. In the present study, we selected a biodegradable polymer coating, poly (lactic-co-glycolic acid), abbreviated as PLGA, to acquire controlled release of icariin from TiO<sub>2</sub> nanotubes [12]. PLGA is the second-generation biomaterials and degradable polymer for biomedical applications, which has attracted great attention due to its outstanding biocompatibility and biodegradability [13]. It can be hydrolyzed into lactic acid and glycolic acid, and the intracorporeal process of Krebs cycle can metabolize these two monomers. Thus, PLGA has been approved by the United States Food and Drug Administration (FDA) and the European Medicines Agency (EMA) for various drug delivery systems in body [14]. In addition, PLGA polymers have the advantage of antibacterial action and enhanced osseointegration properties [15]. In bone tissue engineering, PLGA has been widely used in various forms, such as coatings; fibers; scaffolds etc. Moreover, the Poly (D, L-lactide-coglycolide) 50/50 (Poly 50/50) exhibits faster degradation, which reached 1–2 weeks than other PLGA polymers with different lactic (LA) and glycolic acid (GA) ratios. Thus, we selected Poly 50/50 in order to achieve a relative faster icariin release within the first 2 weeks so that the underlying TiO<sub>2</sub> nanotubes surface may be exposed to exert its osteogenic effect, after the complete release of icariin to promote early osteoblast behaviors [16]. In the present work, we designed to build an icariin-functionalized coating on TiO<sub>2</sub> nanotubes (NT-ICA-PLGA). We hypothesize that the NT-ICA-PLGA surface could prolong the drug release period of icariin. In addition, the icariin-functionalized coating on TiO<sub>2</sub> nanotubes implant surface could promote cell adhesion, proliferation and differentiation in vitro and osseointegration in vivo.

## 2. Materials and Methods

### 2.1. Chemicals and Reagents

Icariin was provided by Shanghai Tauto Biotech Co., Ltd. (Shanghai, China). Resomer®RG 503, PLGA (lactide:glycolide 50:50, ester terminated, *M<sub>w</sub>* 24,000–38,000) was purchased from the Sigma-Aldrich (Sigma-Aldrich Company, St. Louis, MO, USA). Phosphate buffered saline (PBS) was purchased from Hyclone (Logan, UT, USA). Dulbecco's Modified Eagle's Medium - high glucose (D-MEM), fetal bovine serum, penicillin-streptomycin and trypsin were obtained from Thermo Fisher Scientific (Waltham, MA, USA). Cell counting kit-8 (CCK-8) was purchased from Dojindo Molecular Technologies, Inc. (Kumamoto, Japan). Alkaline phosphatase kit was supplied by Jiancheng Co., Ltd (Nanjing, China).

## 2.2. Preparation of TiO<sub>2</sub> Nanotubes

Ti slices (diameter of 15 mm and thickness of 1 mm) were prepared from commercially available pure Ti sheets (ASTM F67 unalloyed Ti grade 2; 99.7% purity; impurities content: Fe—0.09%; C—0.04%; N—0.02%; H—0.008%; O—0.14%; other elements—0.002%), which were obtained from Baoji Titanium Industry (Baoji, China). Ti slices were polished by grit silicon carbide paper of Nos. 600, 800, 1200, then ultrasonically washed with acetone, ethanol, and deionized water for 10 min successively. Subsequently, the slices were dried for 1 h at room temperature. The treated pure titanium was connected to the anode, and platinum was connected to the cathode. The electrolyte consisted of 0.49% HF in deionized water and the reaction voltage was 20 V for 40 min by high voltage DC power supply (Tianjin Dongwen High Voltage Power Supply Factory, Tianjin, China). The titanium plate is used as an anode and platinum sheet as a cathode.

## 2.3. Drug Loading

Icariin solution of 1.15 mg/mL ( $2 \times 10^{-3}$  mol/L) was prepared by dissolving icariin in pure methanol and mixing by vortex oscillators for 2 min. PLGA solution of 13.5 mg/mL was prepared by dissolving PLGA in pure acetone. First, the treated TiO<sub>2</sub> nanotubes sample were immersed in 1 mL icariin solution for 2 days and placed in a drying chamber at 37 °C for 1 day, denoted as the NT-ICA surface. In order to remove the icariin, which loosely attached to the TiO<sub>2</sub> nanotube surface; the prepared NT-ICA samples was washed by 1 mL PBS for 3 times and denoted as NT-ICA (WASH) substrate. Then, 100 µL PLGA solution was dropped to the surface of the NT-ICA sample and allowed for drying naturally. Then, a second 100 µL PLGA solution was dropped again to the dried surface. After drying, the modified surface was named as NT-ICA-PLGA substrate.

## 2.4. Surface Characterization

The surface topography of Ti, Ti-PLGA, NT, NT-ICA and NT-ICA-PLGA surfaces were observed by using scanning electron microscope (S-4800, Hitachi Ltd., Tokyo, Japan). To further observe the composition of icariin-functionalized coating, the icariin and PLGA solutions used in 2.3 were diluted 10 times respectively and uniformly placed dropwise on copper grids (400 mesh size) successively to simulating the preparation process of NT-ICA-PLGA group. After the samples were dried at room temperature, they were examined using transmission electron microscopy (TEM, JEM-2100F; JEOL, Tokyo, Japan). The representative images of three independent experiments were displayed.

The hydrophilicity was assessed through contact angle measurements, which were performed using a contact angle goniometer (JGW-360A, Chongda Intelligent Technology Co., Ltd., Xiamen, China) with 2 µL of deionized water. The data was analyzed by image analysis software (version 1.0, Anglem, Chongda Intelligent Technology Co., Ltd., Xiamen, China). The values were calculated as mean  $\pm$  standard deviation,  $n = 3$ . The experiments were repeated three times.

## 2.5. In Vitro Drug Release Array

The drug concentration in the solution was calculated based on the standard curve. The sample was immersed into 1 mL PBS solution (pH 7.4) in a 24-well plate at 37 °C. At each time point, solution was collected for detection, and then the slices were soaked in 1 mL new PBS solution and measured until the next time point. The supernatant was extracted daily and analyzed with High Performance Liquid Chromatography System (HPLC; 1100 series, Agilent Technologies Ltd, Palo Alto, CA, USA) until 14 days. Icariin concentration was determined from the standard curve. The percentage of drug release was calculated by dividing the cumulated amount of the released drug by the total drug loading amount. Three independent experiments were performed.

## 2.6. Cell Culture

MC3T3-E1 preosteoblast cells (CRL-2593, ATCC, Manassas, VA, USA) was cultured in Dulbecco's Minimum Essential Medium (DMEM, Gibco, Thermo Fisher Scientific, Waltham, MA, USA) with 10% fetal bovine serum (FBS) and 1% penicillin-streptomycin at with 5% CO<sub>2</sub> at 37 °C. The culture medium was refreshed every day.

## 2.7. Cell Morphology

The MC3T3-E1 cells were seeded on the sample surfaces for 24 h at a cell density of  $1 \times 10^4$  cells/mL. Samples were washed by PBS and then fixed with 2.5% glutaraldehyde (Solarbio, Beijing, China) for 40 min at 4 °C. Fixed cells were rinsed twice for 10 min with PBS and followed by dehydration through a gradient ethanol series and critical point drying. After gold sputtering, the cell morphology of samples was observed by scanning electron microscope (S-4800, Hitachi Ltd., Tokyo, Japan). The representative images from three different samples were shown in each group.

## 2.8. Immunofluorescence Staining of Actin Cytoskeleton and Vinculin

All samples (Ti, Ti-PLGA, NT, NT-ICA and NT-ICA-PLGA) were sterilized under the 25 kGy dose of gamma radiation (cobalt-60) (Huanming Gaoke Fuzhao Co. Ltd., Tianjin, China). Cells were seeded onto all samples at  $1 \times 10^4$  cells per well. After 24 h incubation in growth medium, the samples were rinsed by PBS, to remove non-adherent cells. Cells cultured on the samples were fixed in 4% paraformaldehyde (Solarbio, Beijing, China) and permeabilized with 0.25% Triton X-100 (Solarbio, Beijing, China). All samples were then blocked with 1 mL BlockAid™ blocking solution (Thermo Fisher Scientific, Waltham, MA, USA) for 60 min. A 1:50 dilution of rabbit monoclonal vinculin antibody (Sigma-Aldrich Company, St. Louis, MO, USA), followed by a 1:200 dilution of goat-anti-rabbit FITC-conjugated secondary antibody (Sigma-Aldrich Company, St. Louis, MO, USA), was used for the immunostaining of vinculin. Actin cytoskeleton was stained with rhodamine-phalloidin (Thermo Fisher Scientific, Waltham, MA, USA), and nuclei were imaged using 4', 6'-diamidino-2-phenylindole (DAPI; Thermo Fisher Scientific, Waltham, MA, USA). The cells were examined through confocal laser scanning microscopy (CLSM; LSM-800, Carl Zeiss Jena GmbH, Oberkochen, Germany). Three separate substrates were used for each group. The most representative image of three independent experiments was displayed.

## 2.9. Cell Proliferation

Cell proliferation was determined by using cell counting kit-8 (CCK-8) in according with the manufacturer's instructions (Dojindo Molecular Technologies Inc., Kumamoto, Japan). Cells were cultured in all samples at a density of  $1 \times 10^4$  cells/well. After 1, 3, 5 and 7 days, original cell culture medium was removed from different plates, after washed with PBS, 300 µL fresh medium with 30 µL CCK-8 solution was added to each plate. Then, different samples were incubated for 1.5 h at 37 °C and 100 µL of the culture medium were transferred to a new 96-well plate. The absorbance of each well was measured at 450 nm using a microplate reader (Cytation 5, Bio-tek, Winooski, VT, USA). The values were calculated as mean ± standard deviation,  $n = 3$ . The experiments were repeated three times.

## 2.10. Alkaline Phosphatase Activity

MC3T3-E1 cells were seeded onto samples at  $1 \times 10^4$  cells per well in 24-well plate and cultured in the medium for 3, 5, 7 and 14 days. Subsequently, alkaline phosphatase (ALP) activity was evaluated using ALP activity kit (Jiancheng Co., Ltd., Nanjing, China). The alkaline phosphatase activity was determined by reading the absorption value at 520 nm using a microplate reader (Cytation 5, Bio-tek, Winooski, VT, USA). The values were calculated as mean ± standard deviation,  $n = 3$ . The experiments were performed three times.

### 2.11. Animal Experiment

Animal experiments in this study were approved by the Animal Ethics Welfare Committee (AEWC) of Tianjin Medical University (approval no. TMUaMEC 2018003). Twenty-four 12-week-old male Sprague-Dawley (SD) rats (3 rats/group/time point,  $n = 3$ ) were purchased from Model Animal Center of Radiological Medicine Research Institute, Chinese Academy of Medical Science and acclimated for 7 days prior to initiation of studies. The animals were sacrificed two and four weeks after implantation for histological analysis. Animals were housed at 25 °C with a humidity of 55%, and allowed free access to tap water and standard rodent food on a 12-h alternating light-dark cycle. The animals were assigned randomly to four groups: Ti; NT; NT-ICA; NT-ICA-PLGA. Animals were anesthetized by intraperitoneal administration of sodium pentobarbital (50 mg per kg body weight) and supplemental local anesthesia was achieved using lidocaine 2% with epinephrine (1:100000). Ti rods (ASTM F67 unalloyed Ti grade 2) were provided by Baoji Titanium Industry (Baoji, China), and cut into cylindrical implants (diameter of 1.5 mm and heightness of 2 mm). Images of implants used for animal experiments were shown in Figure 1. The pure Ti implants were cleaned and denoted as Ti group. The preparation of NT, NT-ICA, NT-ICA-PLGA groups refers to 2.2 and 2.3. The right hind limbs of rats were shaved, and the skin and muscle tissues were then incised. The mid-diaphysis of the femora was exposed. After that, a hole of 1.5 mm in diameter was drilled with a rotary drill cooled with sterile saline solution. The implants of the Ti, NT, NT-ICA and NT-ICA-PLGA groups were separately implanted into the femora of rats. After that, the skin and muscle tissues were cleaned and sutured. The animals observed no alterations in walking after operation.

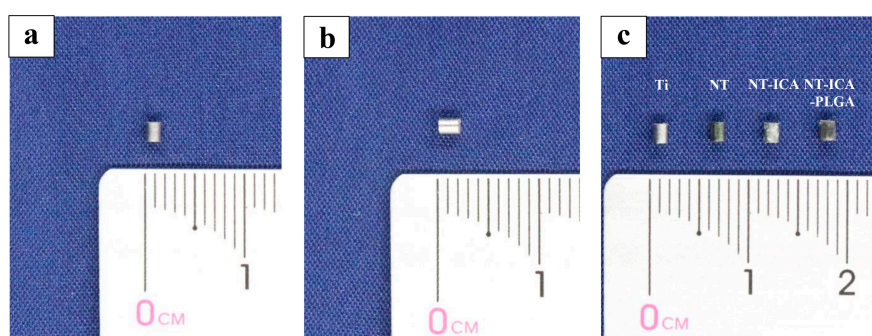


**Figure 1.** Images of implants: (a) Cylindrical pure Ti implant, 1.5 mm in diameter; (b) Cylindrical pure, 2 mm in length; (c) The implants of the Ti, NT, NT-ICA and NT-ICA-PLGA groups. Abbreviations: NT, TiO<sub>2</sub> nanotubes; NT-ICA, TiO<sub>2</sub> nanotubes loading icariin; NT-ICA-PLGA, icariin-functionalized coating on TiO<sub>2</sub> nanotubes surface. The most representative images of three independent experiments were displayed.

SD rats were sacrificed via injecting overdose of sodium pentobarbital two and four weeks after implantation, respectively. Then the femora containing implants were collected, surrounding soft tissue removed and immediately fixed in 10% formalin solution (Solarbio, Beijing, China) for 48 h. After that, all samples were decalcified in 10% ethylenediaminetetraacetic acid (EDTA) (Solarbio, Beijing, China) for 30 days, during which the decalcification solution was replaced every 2 days. When the femora become soft and elastic which can be pierced by needle with no great resistance, the cylindrical implants were carefully taken out by tweezers; leaving the remaining soft tissue around the implant for further histological analysis.

### 2.12. Histological Analysis

All samples were dehydrated using graded ethanol, embedded in paraffin for section preparation. Subsequently, 4 μm thick sections were produced, mounted on glass slides, and stained by hematoxylin and eosin (Solarbio, Beijing, China). Moreover, the sections were observed and photographed by an optical microscope with a digital camera (NI-E, Nikon, Tokyo, Japan). Three fields of view were

pictured at random for each section and three different sections from three different experimental replicates were observed for each group. The most representative images were displaced in each group. Bone apposition analysis was conducted to determine the percentage of new bone formation in designated areas based on H&E staining sections. Image analysis software (Image Pro-Plus 6.0; Media Cybernetics, Silver Spring, MD, USA) were used and the results were shown as bone formation area percentage (BF%), which was defined as the newly formed bone area divided by the defect area extending 100  $\mu\text{m}$  from the implant surface. Five fields of view were photographed at random for each section and three separate sections were calculated for each group.

### 2.13. Statistical Analysis

A one-way ANOVA followed by the Student-Newman-Keuls post hoc test was performed to examine the statistical significance between different samples. Data were reported as mean  $\pm$  standard deviation of three independent experiments. All differences considered to be significant when  $p < 0.05$ .

## 3. Results

### 3.1. Surface Characterization

We used scanning electron microscopy (SEM, S-4800, Hitachi, Tokyo, Japan) to investigate surface topography of all samples. Figure 2A illustrated that Ti disks revealed a smooth surface after polishing, with only a few scratch marks remaining. For the Ti-PLGA slice, PLGA coating totally covered the original Ti surface, with several wrinkles appeared on the substrate. While after anodic oxidation, nanotubular structure layer was fabricated on the Ti surface and the inner diameter of the nanotubes was  $80 \pm 10$  nm. For the NT-ICA-PLGA substrate, the PLGA coatings fully covered the underlying nanotube structures, with just visible contours of icariin under the coating. Figure 2B displayed that through transmission electron microscopy (TEM) observation; icariin (red arrow) can be effectively combined with PLGA (blue arrow).

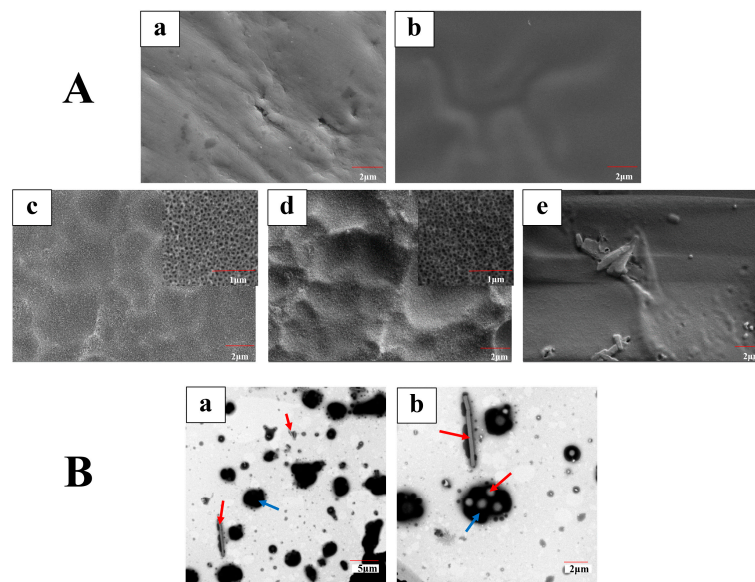


**Figure 2.** (A) Scanning electron microscopy (SEM) images. Images of different surfaces by SEM observed at 5000 $\times$  scale bar, 2  $\mu\text{m}$ : (a) Ti; (b), Ti-PLGA; (c) NT, TiO<sub>2</sub> nanotubes; (d) NT-ICA, TiO<sub>2</sub> nanotubes loading icariin; (e) NT-ICA-PLGA, icariin-functionalized coating on TiO<sub>2</sub> nanotubes surface. Bar indicate 1  $\mu\text{m}$  in magnified insets of (c,d). (B) Images of icariin with poly lactic-co-glycolic acid (PLGA) by transmission electron microscopy (TEM): (a) image observed at 1000 $\times$  scale bar, 5  $\mu\text{m}$ ; (b) image observed at 2000 $\times$ , scale bar, 2  $\mu\text{m}$ . The red arrows denote icariin. The blue arrows denote PLGA. The representative images from three independent experiments were displayed.

As shown in Figure 3, on the non-anodized substrates, the water contact angles were  $89.4^\circ \pm 1.0^\circ$  (Ti) and  $57.7^\circ \pm 1.2^\circ$  (Ti-PLGA), respectively. This suggests that the PLGA coating could increase the hydrophilicity of pure Ti surface. While after anodic oxidation, the contact angles of NT and NT-ICA surfaces decreased to  $36.2^\circ \pm 1.4^\circ$  and  $42.7^\circ \pm 1.5^\circ$ , respectively. This suggests that the  $\text{TiO}_2$  nanotube structure formed by anodic oxidation substantially improved the wettability of surfaces. Moreover, relatively increased contact angles were observed on NT-ICA surfaces ( $42.7^\circ \pm 1.5^\circ$ ) and NT-ICA-PLGA ( $56.3^\circ \pm 1.1^\circ$ ) substrates, as compared to NT ( $36.2^\circ \pm 1.4^\circ$ ) substrate, mainly attributed to the incorporation of icariin and icariin-loaded PLGA coating, respectively. As expected, the contact angle of Ti-PLGA ( $57.7^\circ \pm 1.2^\circ$ ) surface was similar with that of the NT-ICA-PLGA ( $56.3^\circ \pm 1.1^\circ$ ) substrate. It indicates that PLGA coating has completely covered the surfaces of both pure Ti and  $\text{TiO}_2$  nanotube structures in Ti-PLGA and NT-ICA-PLGA groups.

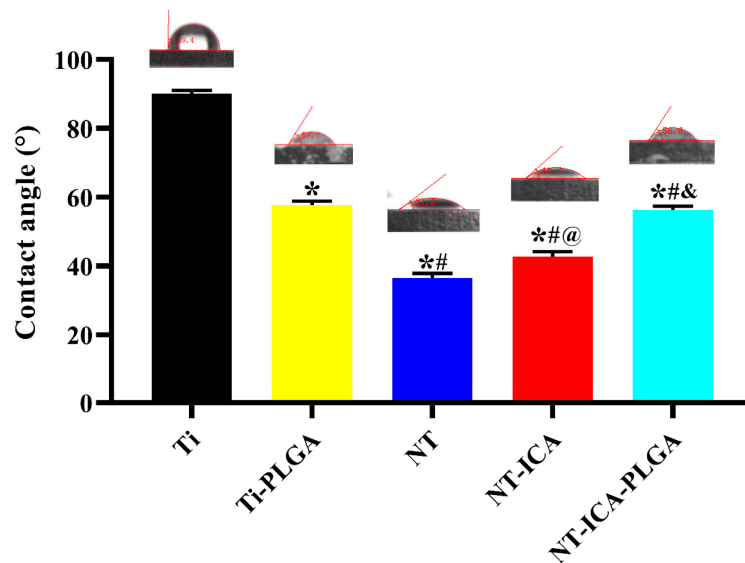


**Figure 3.** Contact angle of different samples. \* indicate statistical significance compared to Ti, # indicate statistical significance compared to Ti-PLGA, @ indicate statistical significance compared to NT and & indicate statistical significance compared to NT-ICA group ( $p < 0.05$ ). The values were calculated as mean  $\pm$  standard deviation,  $n = 3$ . The experiments were repeated three times.

### 3.2. Drug Release

The drug release profile of NT-ICA, NT-ICA (WASH) and NT-ICA-PLGA surfaces was measured for 14 days. Figure 4a showed the release percentage of icariin on different surfaces. A sustained release was observed in NT-ICA-PLGA groups during the 14-day observation period. Both NT-ICA and NT-ICA (WASH) groups reached the plateau at day five and displayed a burst release during the first two days. While the NT-ICA-PLGA surface revealed a much-sustained drug release pattern and higher drug load ability, due to the existence of icariin-loaded PLGA coating. As shown in Figure 4b, the accumulated release amount of icariin follows the sequence of NT-ICA (WASH) < NT-ICA < NT-ICA-PLGA from day 10 to 14.

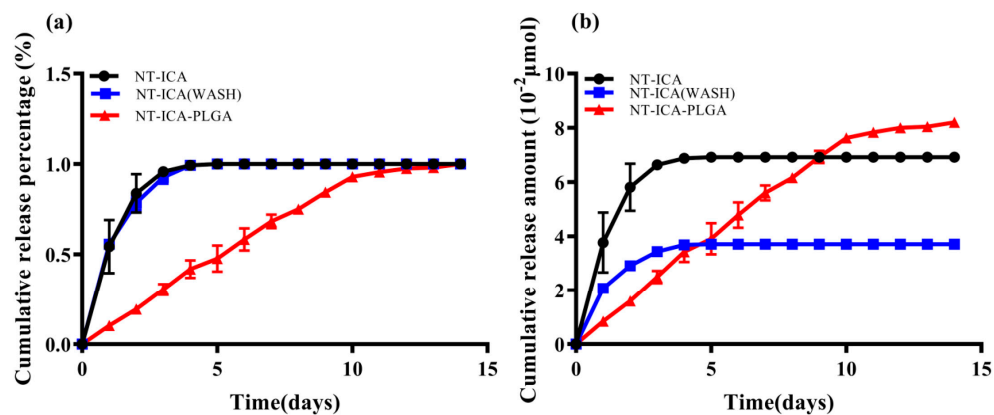


**Figure 4.** In vitro drug release curve of different surfaces. (a) Cumulative release percentage curve; (b) Cumulative release amount curve. Abbreviations: NT-ICA, icariin-loaded  $\text{TiO}_2$  nanotubes; NT-ICA (WASH), icariin-loaded  $\text{TiO}_2$  nanotubes surface, washing out the loosely attached icariin; NT-ICA-PLGA, icariin-functionalized coating on  $\text{TiO}_2$  nanotubes surface. Three independent experiments were performed.

### 3.3. Cell Morphology

Cell adhesion plays a vital role in subsequent cell biological behavior and osseointegration. We observed the cell morphology on different samples by SEM after 24 h of culture. As shown in Figure 5a, osteoblast cells cultured on the original Ti surface spread along the scratch marks produced by polishing. While on the Ti-PLGA, NT and NT-ICA surfaces, cells revealed a spread-out morphology, with several filopodia visible (Figure 5b–d). Moreover, in the MC3T3-E1 cells cultured on the NT-ICA-PLGA substrate, cells exhibited a much well spread morphology, with well-developed filopodia and lamellipodia extending outwards with random orientation, which suggests good cell communication (Figure 5e).

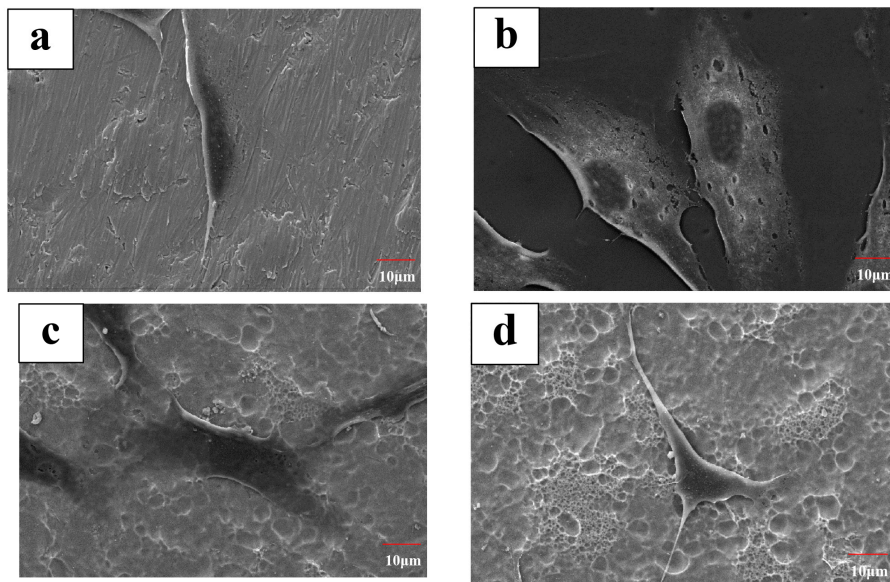


**Figure 5.** Cont.

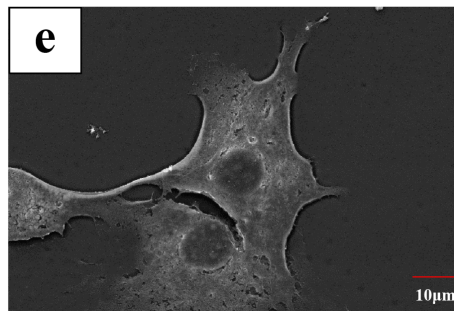


**Figure 5.** Images of MC3T3-E1 cells cultured on different surfaces after 24 h of culture by SEM observed at 1000 $\times$ , scale bar, 10  $\mu\text{m}$ : (a) Ti; (b) Ti-PLGA, pure Ti with PLGA coating; (c) NT, TiO<sub>2</sub> nanotubes; (d) NT-ICA, TiO<sub>2</sub> nanotubes loading icariin; (e) NT-ICA-PLGA, icariin-functionalized coating on TiO<sub>2</sub> nanotubes surface. The representative images of three independent experiments were displayed.

### 3.4. Immunofluorescence of Actin and Vinculin

Osteoblast cells on different samples were further observed by immunofluorescence staining of cytoskeleton actin and vinculin. As shown in Figure 6, on the pure Ti surface, cells tend to extend parallel to the scratch marks, with less actin filament visible. While on the Ti-PLGA, NT and NT-ICA surfaces, cells revealed more actin filaments, which stretched to all directions. In addition, osteoblast cells displayed much more randomly oriented actin filaments stretching out on the NT-ICA-PLGA substrate, suggesting superior cell communication. Meanwhile, the vinculin staining in cells cultured on the modified surfaces displayed stronger fluorescence signal than those on the pristine Ti surface, with the strongest vinculin staining visible in cells on the NT-ICA-PLGA substrate.

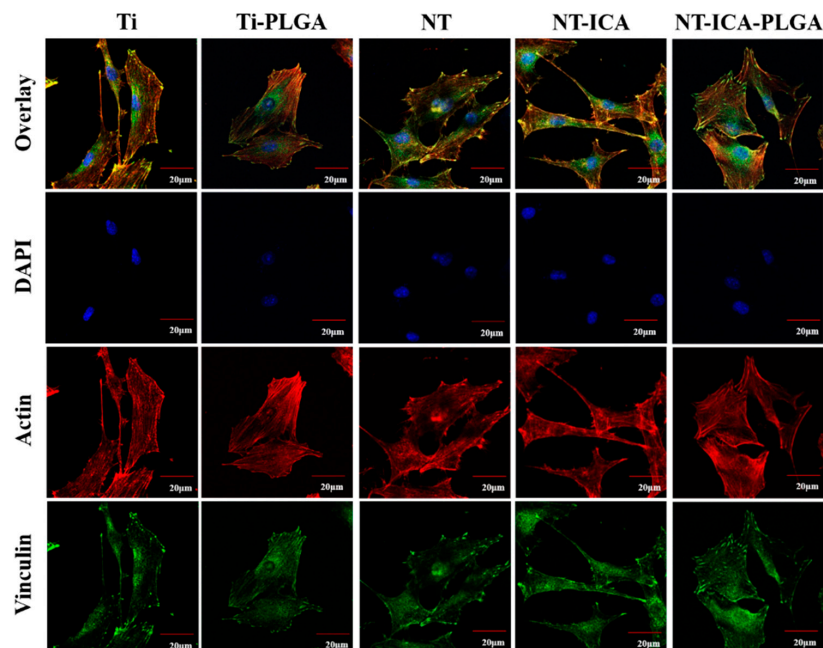


**Figure 6.** Confocal laser scanning microscopy (CLSM) images of MC3T3-E1 cells cultured on the different surfaces after 24 h of incubation. Images of cells stained with DAPI to show nuclei (blue), rhodamine-phalloidin to show actin cytoskeleton (red) and immunofluorescence for vinculin (green). Scale bar, 20  $\mu\text{m}$ . Abbreviations: CLSM, confocal laser scanning microscopy; DAPI, 4', 6-diamidino-2-phenylindole. Three separate substrates were used for each group. The most representative images of three independent experiments were displayed.

### 3.5. Cell Proliferation

The proliferation of MC3T3-E1 cells seeded on the surface of all samples was assessed by CCK-8 assay. Figure 7 showed cell numbers cultured on different surfaces after 1, 3, 5 and 7 days of incubation. Results from the CCK-8 assay displayed the tendency of a continuous increase of cell numbers for cells cultivated on all kinds of specimens during the 7-day period. At each denoted time point, cells cultured on NT-ICA-PLGA substrates revealed higher cell proliferation compared with that on the pristine Ti,  $p < 0.05$ . Meanwhile, cells incubated with the NT-ICA-PLGA substrate also displayed higher proliferation compared to the other groups, suggesting its best performance in improving cell proliferation.

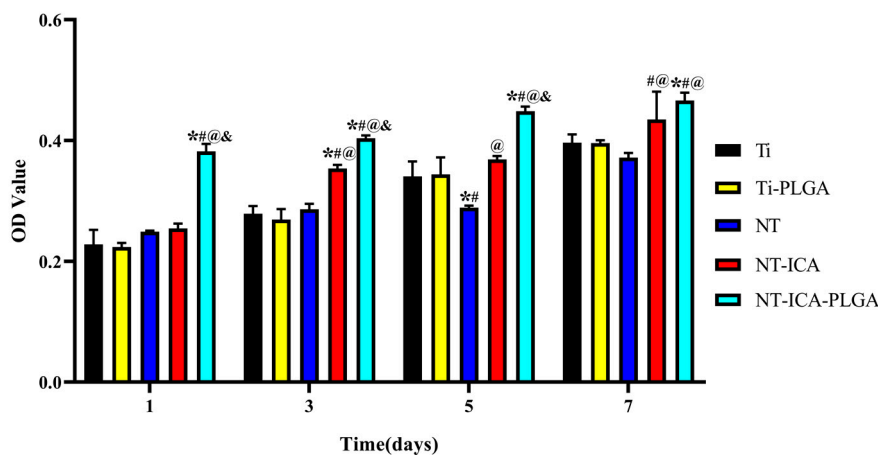


**Figure 7.** CCK-8 assay results of MC3T3-E1 cells on different surfaces after 1, 3, 5, and 7 days. \* indicate statistical significance compared to Ti, # indicate statistical significance compared to Ti-PLGA, @ indicate statistical significance compared to NT and & indicate statistical significance compared to NT-ICA group ( $p < 0.05$ ). The values were calculated as mean  $\pm$  standard deviation,  $n = 3$ . The experiments were repeated three times.

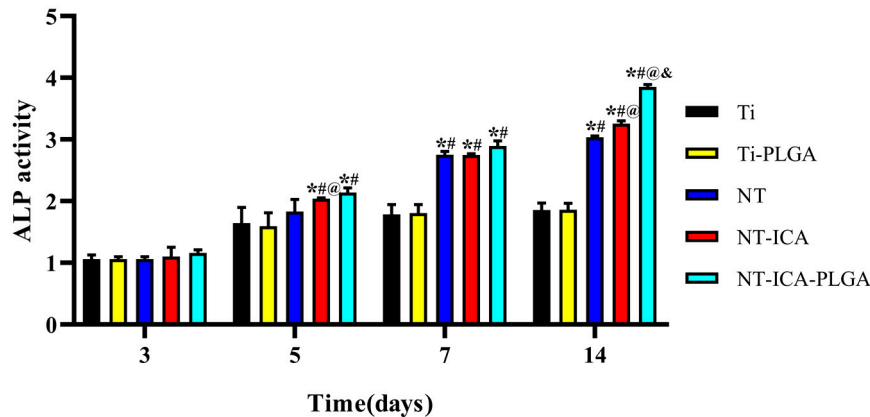
### 3.6. Cell Differentiation

Figure 8 illustrated ALP activity in cells cultured with different samples at 3, 5, 7 and 14 days. As shown in Figure 8, ALP activity gradually increased with time over the 14-day period for all groups. At 7 and 14 days, the ALP activity of cells on the NT, NT-ICA and NT-ICA-PLGA substrates were higher than that cultured on the Ti and Ti-PLGA surfaces ( $p < 0.05$ ). While there is no significant difference between the ALP activity of Ti-PLGA and pure Ti surfaces during the 14-day observation period. More importantly, ALP activity of cells on the NT-ICA-PLGA substrate exhibited much higher ALP activity than all the other surfaces after 14 days of culture, implying its superior ability in promoting osteoblast cell differentiation.

### 3.7. Histological Assessments

Since cell culture tests showed no significant difference between Ti and Ti-PLGA groups in vitro, we removed the Ti-PLGA group to reduce the number of sacrificed animals. At two weeks post-implantation, new bone formation was assessed by H&E staining. It was shown that little newly formed osteoid was seen around the pure Ti implant (Figure 9a). While, more newly formed osteoid were observed in the NT, NT-ICA and NT-ICA-PLGA groups (Figure 9b–d). Especially in the NT-ICA-PLGA group, much more bone trabeculae structures were revealed, suggesting superior bone forming ability than the other groups. Four weeks after implantation, little loosely distributed bone was seen around the implant in the native Ti group, with only a few osteoblasts observed (Figure 9e). On the contrary, relatively well-organized new bone was detected at the tissue-implant interface of the NT, NT-ICA and NT-ICA-PLGA groups (Figure 9f–h). BF% was quantified based on H&E staining of

decalcified sections by bone histomorphometry analysis. Figure 10 showed that BF% of NT-ICA-PLGA group was significantly higher than that of the other groups after 2 weeks of implantation. At 2 weeks, BF% was  $36.63\% \pm 0.8\%$  in the NT-ICA-PLGA group, higher than  $26.5\% \pm 1.2\%$  in the NT-ICA group,  $17.4\% \pm 1.0\%$  in the NT group and  $14.6\% \pm 1.0\%$  in the Ti group ( $p < 0.05$ ). At four weeks post-implantation, BF% was  $49.1\% \pm 3.9\%$  in the NT-ICA-PLGA group,  $45.7\% \pm 3.3\%$  in the NT-ICA group and  $43.2\% \pm 2.5\%$  in the NT group, higher than  $27.2\% \pm 4.8\%$  in the Ti group ( $p < 0.05$ ).



**Figure 8.** ALP activity of MC3T3-E1 cells on different surfaces after 3, 5, 7 and 14 days. \* indicate statistical significance compared to Ti, # indicate statistical significance compared to Ti-PLGA, @ indicate statistical significance compared to NT and & indicate statistical significance compared to NT-ICA group ( $p < 0.05$ ). The values were calculated as mean  $\pm$  standard deviation,  $n = 3$ . The experiments were repeated three times.

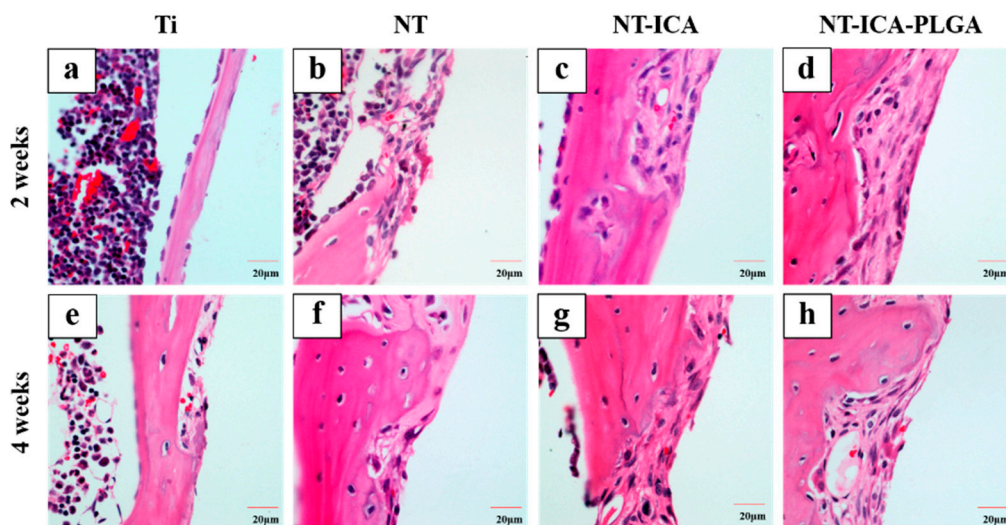


**Figure 9.** Histological analysis of the decalcification samples around different implants was evaluated by H&E staining. Scale bar, 20 $\mu$ m. Ti (a,e); NT (b,f), TiO<sub>2</sub> nanotubes; NT-ICA (c,g), TiO<sub>2</sub> nanotubes loading icariin; NT-ICA-PLGA (d,h), icariin-functionalized coating on TiO<sub>2</sub> nanotubes surface; (a–d) Two weeks after implantation; (e–h) Four weeks after implantation. Three fields of view were pictured at random for each section and three different sections from three different experimental replicates were observed for each group. The most representative images were displaced in each group.

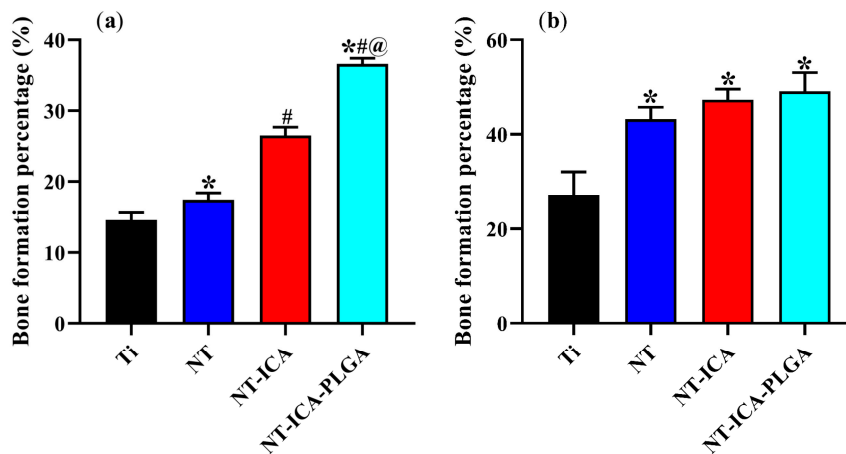


**Figure 10.** Histomorphometric analyses based on H&E staining after 2 and 4 weeks of implantation was expressed in BF %. (a) BF % after 2 weeks of implantation (b) BF % after 4 weeks of implantation. \* indicate statistical significance compared to Ti, # indicate statistical significance compared to NT and @ indicate statistical significance compared to NT-ICA ( $p < 0.05$ ). Abbreviations: NT, TiO<sub>2</sub> nanotubes; NT-ICA, TiO<sub>2</sub> nanotubes loading icariin; NT-ICA-PLGA, icariin-functionalized coating on TiO<sub>2</sub> nanotubes surface. Five fields of view were photographed at random for each section and three separate sections were calculated for each group.

These results displayed that two weeks after implantation, bone formation around the implants of NT-ICA and NT-ICA-PLGA groups was obviously more than that of the Ti and NT groups, suggesting the effect of icariin in the promotion of early osseointegration. In particular, the BF% of the NT-ICA-PLGA group was higher than that of the NT-ICA group, implying its superior bone formation ability by the controlled release of icariin from the functionalized surface. At four weeks after implantation, the NT, NT-ICA and NT-ICA-PLGA groups displayed higher BF% than the pristine Ti group, whereas there was no significant difference between NT, NT-ICA and NT-ICA-PLGA groups. This is probably explained by the completely release of icariin during the initial 14 days, which narrowed the gap of osteogenic effects between NT, NT-ICA and NT-ICA-PLGA groups after two weeks. It is speculated that the nanotube structure began to promote bone formation after two weeks of implantation. These results indicated that the icariin-functionalized coating on TiO<sub>2</sub> nanotubes work most effectively during the initial two weeks to accelerate early osseointegration in vivo.

#### 4. Discussion

In the present study, we successfully established an icariin-functionalized coating on TiO<sub>2</sub> nanotubes surface, which could combine the TiO<sub>2</sub> nanotubes structure with osteogenic drug icariin. The outer PLGA coverage endowed the functionalized icariin-loaded coating with sustained drug release ability until two weeks after implantation. In the icariin-functionalized coating on TiO<sub>2</sub> nanotubes surface, the nano-scale surface morphology and osteogenic drug icariin could exert synergistic effects to improve biocompatibility in cell culture tests and accelerate osseointegration in animal model as well.

Icariin, the traditional Chinese medicine, displayed strong antiapoptotic abilities in osteocytes under osteoporotic conditions and has a potential osteogenic function [17]. Moreover, icariin was easy to store and has an ideal stability, which was not affected by radiation or heating [18]. It has been reported that nearly 90% of currently used drugs in implant modification are hydrophobic, and icariin is no exception [19]. That said, icariin has a number of shortcomings, such as the first-pass effect after oral administration and low bioavailability, which limit its clinical application [20]. Previous studies have shown that icariin could be combined with small intestine submucosa scaffold to enhance bone regeneration [21]. Icariin was also incorporated into bioactive glass based scaffolds coated with gelatin for the sustained release of icariin [22]. In addition, precious results also demonstrated that

icariin could be conjugated with nanofiber hydrogel scaffolds to promote chondrogenic differentiation of bone marrow mesenchymal stem cells [23]. In summary, previous reports mostly focus on the usage of icariin in bone tissue-engineering scaffold or the cartilage [24] or osteochondral interface restoration [25]. However, polymer-scaffolding materials are not suitable for dental implants because of strength issues. In addition, dental implants are typically made of titanium material, which could promote the stable and functional connection between bone tissue and implant surface [26].

To solve the problems mentioned above, this work aims to combine the mechanical rigidity, bioactivity, and drug delivery capability—to establish an ICA-functionalized coating on the titanium implant material for orthopedic and dental applications. On one hand, the locally applied ICA-functionalized coating could avoid the side effects caused by the systemic administration of drugs. On the other hand, we employed the TiO<sub>2</sub> nanotubes structure as a drug reservoir to achieve the gradual and controlled release of icariin, which may impede the side effects caused by burst release, increase the local effectiveness, and optimize the bioavailability as well.

Anodic oxidation is an economic and effective method to obtain a TiO<sub>2</sub> nanotube structure on the implant surface. The prepared TiO<sub>2</sub> nanotubes have potential drug delivery capabilities and could facilitate osteoblast (bone-forming cell) adhesion and improve the subsequent cell functions [27]. It is reported that TiO<sub>2</sub> nanotubes with a small diameter (about 30 nm) could promote cell adhesion, and those with a diameter of 70–100 nm could induce cell elongation, which eventually led to the transformation in cytoskeletal stress and the differentiation toward osteoblasts [28,29]. Studies also showed that cell adhesion, alkaline phosphatase activity and mineralization are severely impaired on the 100–120 nm nanotube layer [30]. Moreover, TiO<sub>2</sub> nanotubes with a diameter of 80 nm decreased the adhesion of both dead and live bacteria for both *Staphylococcus epidermidis* and *Staphylococcus aureus*, providing the most robust antibacterial effect [31]. In addition, relative larger diameter of TiO<sub>2</sub> nanotubes generally implies better drug loading ability. Based on the above-mentioned reports, in the present study, we focused on the balance among drug loading ability, effects on cell biological behaviors and antibacterial function when determining the size of TiO<sub>2</sub> nanotubes. Finally, we brought forward a feasible solution by using the 80nm diameter TiO<sub>2</sub> nanotubes, which not only obtains an ideal drug delivery system for icariin release, but also satisfied biocompatibility for cells and possesses potential better antibacterial activity, which will be further studied in the future.

Apart from the drug reservoir of TiO<sub>2</sub> nanotubes layer, a local controlled and sustained drug delivery system is also needed to avoid drug toxicity caused by burst release and extend the duration of the drug's action [32]. Among the various coating materials, PLGA is well accepted for its good degradability and strong drug-loading capacity compared with chitosan when used as a scaffold material [33,34]. The previous study showed that TiO<sub>2</sub> nanotubes coated with a PLGA polymer layer have extended release duration and higher level of burst release than TiO<sub>2</sub> nanotubes coated with chitosan [35]. Therefore, in the present work, in order to further prolong the drug release period, we further superimposed the PLGA coating on the TiO<sub>2</sub> nanotubes structure to obtain sustained release of ICA on the functionalized coating.

In addition, Poly 50/50 was used because it has rapid degradation ability to ensure the underlying nanotubes topography could be gradually exposed to exert its osteogenic effects two weeks after implantation. The established NT-ICA-PLGA surface prolonged the drug release period until 14 days from the original five days of the NT-ICA group. Meanwhile, the cumulative release curve of NT-ICA-PLGA indicate that icariin-functionalized coating can maintain the controlled drug release profile and a nearly linearly increasing cumulative release trend over a period of the initial 10 days.

More importantly, the established NT-ICA-PLGA functionalized surface successfully inhibited the burst release and related toxic effect of icariin during the initial 2–3 days of drug release. In addition, the icariin-functionalized coating also ensured sustained drug release of icariin to exert its osteogenic effect throughout the first 14 days post-implantation, which is regarded as a critical period of early osseointegration [36]. Moreover, increased hydrophilicity may have directly accelerated cell proliferation and differentiation of preosteoblast cells by promoting the related signal pathways,

such as Wnt, Notch, TGF- $\beta$  pathways, etcetera [37]. The increased wettability of the NT-ICA-PLGA functionalized surface may also explain its superior biocompatibility for osteoblast cells behaviors in vitro and osseointegration in vivo.

In order to verify the effect of different samples on cells, we chose the MC3T3-E1 mouse preosteoblastic cells, which have been widely used as cell model systems in bone biology, for in vitro tests in this study. It is shown that osteoblast cells cultured on the Ti sample displayed cell morphology pattern which stretched parallel along the polishing marks; while cells adhered to the Ti-PLGA, NT and NT-ICA surfaces revealed advanced cell adhesion properties, with randomly arranged directions. Moreover, osteoblast cells attached best on the NT-ICA-PLGA substrate, with many stretched filopodia indicating advanced cell communication. These results suggest that both PLGA and nanotube structures could promote cell adhesion. Interestingly, the incorporation of icariin-loaded PLGA and nanoscale surface topography could play a synergistic role in promoting osteoblast cells adhesion.

CCK-8 kit is a convenient reagent, which allows sensitive colorimetric assays for the determination of the number of viable cells in cell activity, cell proliferation and cytotoxicity assays. The higher the OD value, the higher the activity and proliferation ability of living cells. CCK-8 test showed that the number of cells on different substrates generally increased with seeding time during the 7-day observation period. The NT-ICA-PLGA group showed the best proliferative capacity than other groups. In addition, cells cultured on the Ti-PLGA group revealed similar cell viability compared to the Ti group. Our results indicated that PLGA coatings exhibited no cytotoxicity. Some studies have shown that low dose ( $10^{-7}$ ,  $10^{-8}$ ,  $10^{-9}$  mol/L) of icariin could promote cell proliferation, while high dose ( $10^{-5}$ ,  $10^{-6}$  mol/L) of icariin promote cell differentiation of MC3T3-E1 cells [38,39]. However the best concentration was not clear. The drug release curve indicated that the concentration of released icariin was maintained at  $10^{-5}$  mol/L in NT-ICA-PLGA group during the initial 10 days. Our results showed that relatively high doses of icariin could promote early cell proliferation during the first seven days.

Alkaline phosphatase is used as a marker for early differentiation of osteoblast [40]. Our data showed that ALP activity of MC3T3-E1 cells on NT, NT-ICA and NT-ICA-PLGA substrates were higher than that of the original Ti group. This result is in accordance with previous literature, which showed that the increased ALP activity on all groups from day three to day 14 is ascribed to the continuous osteoblast differentiation [41]. On day 14, cells on the NT-ICA-PLGA substrate displayed the highest ALP activity compared to the other groups. It may be due to the synergistic action of gradual release of icariin and nano-scale structure formed by the functionalized coating on the TiO<sub>2</sub> nanotube structure. Therefore the highest cell proliferation was observed on the NT-ICA-PLGA substrate. As we know, cell proliferation and differentiation are somewhat antagonistic in cell life activities. When cells are strongly differentiated, proliferative activity is inhibited, and vice versa [26]. In our study, cells cultured on the NT-ICA-PLGA surface displayed the best proliferation and differentiation capacity at the same time, compared to the other specimens. These results infer that both the TiO<sub>2</sub> nanotube structure and functionalized icariin-loaded PLGA coating exerted combined effects to improve cell proliferation and differentiation. Moreover, the controlled release of icariin further promotes cell proliferation and differentiation ability of the NT-ICA-PLGA surface.

We also used the rat model to explore the osteogenic effects of different implant surfaces in vivo. The results showed that compared with the other groups, the NT-ICA-PLGA functionalized substrate displayed the best bone forming ability, with higher BF% than the other groups during the early-stage of osseointegration. The abovementioned results showed that both nanoscale structure and icariin could improve the growth of new bone at the early stage after implantation. Importantly, the significantly improved bone formation capacity was observed in the NT-ICA-PLGA functionalized substrate. It suggested that sustained release of icariin with appropriate concentration of the NT-ICA-PLGA group could acquire the best osteogenic effects by accelerating the bone mineralization rate around the implant, in order to improve the early stability of the implant.

## 5. Conclusions

In the present work, we established the icariin-functionalized coating on TiO<sub>2</sub> nanotubes surface (NT-ICA-PLGA). In addition, The NT-ICA-PLGA surface could refrain from the burst release of icariin and achieve the sustained release of icariin to as long as two weeks. The in vitro results revealed that both TiO<sub>2</sub> nanotubes and icariin could promote osteoblast cell adhesion, proliferation and differentiation much better than the as-polished titanium surface in vitro. Furthermore, in vivo experiments also confirmed that NT-ICA-PLGA modified substrate has better osteogenic ability on implant/bone interface than TiO<sub>2</sub> nanotube layer alone or original Ti substrate. Therefore, our results implied that the nanotubes structure and icariin could synergistically promote osteoblast cell function and improve osseointegration. In addition, the NT-ICA-PLGA modified surface could further enhance the osteogenic effects by the additional PLGA coating, which endowed the functionalized coating with slow and steady drug release ability for icariin. In summary, our results suggested a very promising applicable future for the newly established icariin-functionalized coating on TiO<sub>2</sub> nanotubes surface.

**Author Contributions:** Conceptualization, C.L., Y.L. and X.Z.; Data Curation, A.M., H.S., W.H. and W.Z.; Funding Acquisition, C.L. and Y.L.; Investigation, A.M., H.S., Y.S., B.C. and Y.Y.; Methodology, A.M., H.S. and Y.S.; Project Administration, C.L. and Y.L.; Writing—Original Draft, A.M.; Writing—Review and Editing, Y.L.

**Funding:** This study was supported by grants from National Natural Science Foundation of China (Nos. 81870809, 81500886, 31470920), Tianjin Natural Science Foundation (No. 16JCYBJC28700) and Natural Science Foundation of Hebei Province of China (No. E2017202032).

**Acknowledgments:** We sincerely acknowledge Baoye Li from the School of Materials Science and Engineering, Hebei University of Technology, for her precious technical support and discussions. We also thank Huanhuan Zhai from Tianjin Institute of Industrial Biotechnology, Chinese Academy of Sciences, for her important work in preparing SEM images.

**Conflicts of Interest:** The authors declare that there are no conflict of interest regarding the publication of this paper.

## References

1. Kulkarni, M.; Mazare, A.; Gongadze, E.; Perutkova, S.; Kralj-Iglic, V.; Milosev, I.; Schmuki, P.; Iglic, A.; Mozetic, M. Titanium nanostructures for biomedical applications. *Nanotechnology* **2015**, *26*, 062002. [[CrossRef](#)] [[PubMed](#)]
2. Rani, V.V.; Vinoth-Kumar, L.; Anitha, V.C.; Manzoor, K.; Deepthy, M.; Shantikumar, V.N. Osteointegration of titanium implant is sensitive to specific nanostructure morphology. *Acta Biomater.* **2012**, *8*, 1976–1989. [[CrossRef](#)] [[PubMed](#)]
3. Dohan Ehrenfest, D.M.; Coelho, P.G.; Kang, B.S.; Sul, Y.T.; Albrektsson, T. Classification of osseointegrated implant surfaces: Materials, chemistry and topography. *Trends Biotechnol.* **2010**, *28*, 198–206. [[CrossRef](#)]
4. Shan, L.; Kadhum, A.A.H.; Al-Furjan, M.S.H. In situ controlled surface microstructure of 3d printed Ti alloy to promote its osteointegration. *Materials* **2019**, *12*, 815. [[CrossRef](#)]
5. Vyatskikh, A.; Delalande, S.; Kudo, A.; Zhang, X.; Portela, C.M.; Greer, J.R. Additive manufacturing of 3d nano-architected metals. *Nat. Commun.* **2018**, *9*, 3864–3870. [[CrossRef](#)] [[PubMed](#)]
6. Losic, D.; Simovic, S. Self-ordered nanopore and nanotube platforms for drug delivery applications. *Expert Opin. Drug Deliv.* **2009**, *6*, 1363–1381. [[CrossRef](#)]
7. Roy, P.; Berger, S.; Schmuki, P. TiO<sub>2</sub> nanotubes: Synthesis and applications. *Angew. Chem. Int. Ed. Engl.* **2011**, *50*, 2904–2939. [[CrossRef](#)] [[PubMed](#)]
8. Stan, M.S.; Memet, I.; Fratila, C.; Krasicka-Cydzik, E.; Roman, I.; Dinischiotu, A. Effects of titanium-based nanotube films on osteoblast behavior in vitro. *J. Biomed. Mater. Res. Part A* **2015**, *103*, 48–56. [[CrossRef](#)]
9. Yu, W.; Qian, C.; Jiang, X.; Zhang, F.; Weng, W. Mechanisms of stem cell osteogenic differentiation on TiO<sub>2</sub> nanotubes. *Colloids Surf. Biointerfaces* **2015**, *136*, 779–785. [[CrossRef](#)] [[PubMed](#)]
10. Zhang, X.; Liu, T.; Huang, Y.; Wismeijer, D.; Liu, Y. Icariin: Does it have an osteoinductive potential for bone tissue engineering? *Phytother. Res.* **2014**, *28*, 498–509. [[CrossRef](#)] [[PubMed](#)]
11. Zhao, J.; Ohba, S.; Komiyama, Y.; Shinkai, M.; Chung, U.I.; Nagamune, T. Icariin: A potential osteoinductive compound for bone tissue engineering. *Tissue Eng. Part A* **2010**, *16*, 233–243. [[CrossRef](#)]

12. Losic, D.; Aw, M.S.; Santos, A.; Gulati, K.; Bariana, M. Titania nanotube arrays for local drug delivery: Recent advances and perspectives. *Expert Opin. Drug Deliv.* **2015**, *12*, 103–127. [[CrossRef](#)] [[PubMed](#)]
13. Anderson, J.M.; Shive, M.S. Biodegradation and biocompatibility of PLA and PLGA microspheres. *Adv. Drug Deliv. Rev.* **1997**, *28*, 5–24.
14. Kumari, A.; Yadav, S.K.; Yadav, S.C. Biodegradable polymeric nanoparticles based drug delivery systems. *Colloids Surf. Biointerfaces* **2010**, *75*, 1–18. [[CrossRef](#)] [[PubMed](#)]
15. Sun, S.; Zhang, Y.; Zeng, D.; Zhang, S.; Zhang, F.; Yu, W. PLGA film/titanium nanotubes as a sustained growth factor releasing system for dental implants. *J. Mater. Sci. Mater. Med.* **2018**, *29*, 141. [[CrossRef](#)] [[PubMed](#)]
16. Gentile, P.; Chiono, V.; Carmagnola, I.; Hatton, P.V. An overview of poly(lactic-co-glycolic) acid (PLGA)-based biomaterials for bone tissue engineering. *Int. J. Mol. Sci.* **2014**, *15*, 3640–3659. [[CrossRef](#)] [[PubMed](#)]
17. Feng, R.; Feng, L.; Yuan, Z.; Wang, D.; Wang, F.; Tan, B.; Han, S.; Li, T.; Li, D.; Han, Y. Icaritin protects against glucocorticoid-induced osteoporosis in vitro and prevents glucocorticoid-induced osteocyte apoptosis in vivo. *Cell Biochem. Biophys.* **2013**, *67*, 189–197. [[CrossRef](#)] [[PubMed](#)]
18. Wu, T.; Nan, K.; Chen, J.; Jin, D.; Jiang, S.; Zhao, P.; Xu, J.; Du, H.; Zhang, X.; Li, J.; et al. A new bone repair scaffold combined with chitosan/ hydroxyapatite and sustained releasing icaritin. *Chin. Sci. Bull.* **2009**, *54*, 2953–2961. [[CrossRef](#)]
19. Aw, M.S.; Kurian, M.; Losic, D. Non-eroding drug-releasing implants with ordered nanoporous and nanotubular structures: Concepts for controlling drug release. *Biomater. Sci.* **2014**, *2*, 10–34.
20. Sun, X.; Wei, J.; Lyu, J.; Bian, T.; Liu, Z.; Huang, J.; Pi, F.; Li, C.; Zhong, Z. Bone-targeting drug delivery system of biomineral-binding liposomes loaded with icaritin enhances the treatment for osteoporosis. *J. Nanobiotechnol.* **2019**, *17*, 10. [[CrossRef](#)] [[PubMed](#)]
21. Yin, L.; Wang, K.; Lv, X.; Sun, R.; Yang, S.; Yang, Y.; Liu, Y.; Liu, J.; Zhou, J.; Yu, Z. The fabrication of an ica-sf/plcl nanofibrous membrane by coaxial electrospinning and its effect on bone regeneration in vitro and in vivo. *Sci. Rep.* **2017**, *7*, 8616. [[CrossRef](#)] [[PubMed](#)]
22. Reiter, T.; Panick, T.; Schuhladen, K.; Roether, J.A.; Hum, J.; Boccaccini, A.R. Bioactive glass based scaffolds coated with gelatin for the sustained release of icaritin. *Bioact. Mater.* **2019**, *4*, 1–7. [[CrossRef](#)] [[PubMed](#)]
23. Wang, Z.; Li, K.; Sun, H.; Wang, J.; Fu, Z.; Liu, M. Icaritin promotes stable chondrogenic differentiation of bone marrow mesenchymal stem cells in self-assembling peptide nanofiber hydrogel scaffolds. *Mol. Med. Rep.* **2018**, *17*, 8237–8243. [[CrossRef](#)] [[PubMed](#)]
24. Kankala, R.K.; Lu, F.J.; Liu, C.G. Effect of icaritin on engineered 3d-printed porous scaffolds for cartilage repair. *Materials* **2018**, *11*, 1390. [[CrossRef](#)] [[PubMed](#)]
25. Yang, J.; Liu, Y.; He, L.; Wang, Q.; Wang, L.; Yuan, T.; Xiao, Y.; Fan, Y.; Zhang, X. Icaritin conjugated hyaluronic acid/collagen hydrogel for osteochondral interface restoration. *Acta Biomater.* **2018**, *74*, 156–167. [[CrossRef](#)] [[PubMed](#)]
26. Schmitt, B.; Ringe, J.; Haupl, T.; Notter, M.; Manz, R.; Burmester, G.R.; Sittinger, M.; Kaps, C. Bmp2 initiates chondrogenic lineage development of adult human mesenchymal stem cells in high-density culture. *Differ. Res. Biol. Divers.* **2003**, *71*, 567–577. [[CrossRef](#)]
27. Song, Y.Y.; Schmidt-Stein, F.; Bauer, S.; Schmuki, P. Amphiphilic TiO<sub>2</sub> nanotube arrays: An actively controllable drug delivery system. *J. Am. Chem. Soc.* **2009**, *131*, 4230–4232. [[CrossRef](#)] [[PubMed](#)]
28. Lai, Y.; Yan, C.; Hui, Y.; Yun, Y.; Lin, C. Progress in TiO<sub>2</sub> nanotube coatings for biomedical applications: A review. *J. Mater. Chem. B* **2018**, *6*, 1862–1886.
29. Von Wilmowsky, C.; Bauer, S.; Roedel, S.; Neukam, F.W.; Schmuki, P.; Schlegel, K.A. The diameter of anodic TiO<sub>2</sub> nanotubes affects bone formation and correlates with the bone morphogenetic protein-2 expression in vivo. *Clin. Oral Implant. Res.* **2012**, *23*, 359–366. [[CrossRef](#)]
30. Yu, W.Q.; Jiang, X.Q.; Zhang, F.Q.; Xu, L. The effect of anatase TiO<sub>2</sub> nanotube layers on MC3T3-E1 preosteoblast adhesion, proliferation, and differentiation. *J. Biomed. Mater. Res. A* **2010**, *94*, 1012–1022. [[CrossRef](#)]
31. Ercan, B.; Taylor, E.; Alpaslan, E.; Webster, T.J. Diameter of titanium nanotubes influences anti-bacterial efficacy. *Nanotechnology* **2011**, *22*, 295102. [[CrossRef](#)] [[PubMed](#)]
32. Wu, P.; Grainger, D.W. Drug/device combinations for local drug therapies and infection prophylaxis. *Biomaterials* **2006**, *27*, 2450–2467. [[CrossRef](#)] [[PubMed](#)]

33. Lai, Y.; Cao, H.; Wang, X.; Chen, S.; Zhang, M.; Wang, N.; Yao, Z.; Dai, Y.; Xie, X.; Zhang, P.; et al. Porous composite scaffold incorporating osteogenic phytomolecule icariin for promoting skeletal regeneration in challenging osteonecrotic bone in rabbits. *Biomaterials* **2018**, *153*, 1–13. [[CrossRef](#)]
34. Qin, L.; Yao, D.; Zheng, L.; Liu, W.C.; Liu, Z.; Lei, M.; Huang, L.; Xie, X.; Wang, X.; Chen, Y.; et al. Phytomolecule icaritin incorporated plga/tcp scaffold for steroid-associated osteonecrosis: Proof-of-concept for prevention of hip joint collapse in bipedal emus and mechanistic study in quadrupedal rabbits. *Biomaterials* **2015**, *59*, 125–143. [[CrossRef](#)]
35. Wang, Q.; Huang, J.; Li, H.; Zhao, Z.J.; Yi, W.; Zhang, K.Q.; Sun, H.; Lai, Y. Recent advances on smart tio2nanotube platforms for sustainable drug delivery applications. *Int. J. Nanomed.* **2017**, *12*, 151–165. [[CrossRef](#)]
36. Offermanns, V.; Andersen, O.Z.; Sillassen, M.; Almtoft, K.P.; Andersen, I.H.; Kloss, F.; Foss, M. A comparative in vivo study of strontium-functionalized and slactive™ implant surfaces in early bone healing. *Int. J. Nanomed.* **2018**, *13*, 2189–2197. [[CrossRef](#)]
37. Calciolari, E.; Hamlet, S.; Ivanovski, S.; Donos, N. Pro-osteogenic properties of hydrophilic and hydrophobic titanium surfaces: Crosstalk between signalling pathways in in vivo models. *J. Periodontal. Res.* **2018**, *53*, 598–609. [[CrossRef](#)] [[PubMed](#)]
38. Liu, H.; Li, W.; Luo, B.; Chen, X.; Wen, W.; Zhou, C. Icariin immobilized electrospinning poly(l-lactide) fibrous membranes via polydopamine adhesive coating with enhanced cytocompatibility and osteogenic activity. *Mater. Sci. Eng. C Mater. Biol. Appl.* **2017**, *79*, 399–409. [[CrossRef](#)]
39. Liu, Y.; Huang, L.; Hao, B.; Li, H.; Zhu, S.; Wang, Q.; Li, R.; Xu, Y.; Zhang, X. Use of an osteoblast overload damage model to probe the effect of icariin on the proliferation, differentiation and mineralization of mc3t3-e1 cells through the wnt/beta-catenin signalling pathway. *Cell. Physiol. Biochem. Int. J. Exp. Cell. Physiol. Biochem. Pharmacol.* **2017**, *41*, 1605–1615. [[CrossRef](#)]
40. An, J.; Yang, H.; Zhang, Q.; Liu, C.; Zhao, J.; Zhang, L.; Chen, B. Natural products for treatment of osteoporosis: The effects and mechanisms on promoting osteoblast-mediated bone formation. *Life Sci.* **2016**, *147*, 46–58. [[CrossRef](#)]
41. Khudhair, D.; Bhatti, A.; Li, Y.; Hamedani, H.A.; Garmestani, H.; Hodgson, P.; Nahavandi, S. Anodization parameters influencing the morphology and electrical properties of TiO<sub>2</sub> nanotubes for living cell interfacing and investigations. *Mater. Sci. Eng. C Mater. Biol. Appl.* **2016**, *59*, 1125–1142. [[CrossRef](#)]



© 2019 by the authors. Licensee MDPI, Basel, Switzerland. This article is an open access article distributed under the terms and conditions of the Creative Commons Attribution (CC BY) license (<http://creativecommons.org/licenses/by/4.0/>).